Self-exothermic esterification-crosslinking of bio-polymer/graphene composite for application in interbody fusion cage

Kangtai Ou[1], Qingxiao Liu[1], Xiaodong Liu[2*], Qiang Fu[1, 3], Jiang Fan[1], Youyi Sun[1*]

[1]School of materials science and technology, North University of China, Taiyuan 030051, P.R. China.
[2]Department of Neurosurgery, First Hospital of Shanxi Medical University, 85 Jiefang Road, Taiyuan, Shanxi 030001, P.R. China
[3]School of Civil and Environmental Engineering, University of Technology Sydney, Ultimo NSW 2007, Australia.

Abstract: The commercial interbody fusion cage is generally based on rigid materials (eg. Ti metal, PEEK plastic and so on), resulting in discomfort and limiting the movement of vertebration for human. A new soft and elastic polymer composite is prepared by self-exothermic esterification-crosslinking method for application in interbody fusion cage. It is mainly composed of bio-polymer (eg. PVA and Chitosan), hydroxyapatite and graphene nanosheets. The interbody fusion cage is fabricated by 3D printing and mould process from bio-polymer composite. The interbody fusion cage does not only show high elastic modulus (*ca.* 246.5MPa), but also exhibits good compression elastic deformation (more than 15%), enhancing comfort of human. Furthermore, the interbody fusion cage can produce Ca ions and shows grade 1 (few reactivity) of cytotoxicity, indicating good osteoconductivity and biocompatibility. The work demonstrates the practical application of present bio-polymer/graphene composite in interbody fusion cage with comfort.

Keywords: Scale-up/manufacturing, Biomaterial, Graphene, Composite, Viscoelasticity.

Responding author: Fax: 86-351-3922949
E-mail address: syyi@pku.edu.cn (YY Sun), wuwg2010@163.com (XD Liu)

Introduction

The commercial intervertebral fusion cages are generally fabiricated from these rigid materials, such as poly(etheretherketone) (PEEK), titanium, carbon fiber, polyamide 66 (PA 66) and so on[1-5]. The application of these rigid materials in fusion cage devices still faces three major problems. Firstly, the osteoconductivity of these materials are poor, resulting in lowinterfacial strength between the cage and the bone. Secondly, these materials also show poor biocompatibility, leading to inflammatory reaction between the cage and the bone. Thirdly, these materials are basically rigid and inelastic, causing inflammation and rigid intervertebral for human. To overcome above problmes, hydroxyapatite has attracted considerable attention in intervertebral fusion cages due to its good biocompatibility and osteoconductivity. For example, Shikinami *et al* reported a bioactive, resorbable hydroxyapatite/polyl-lactide (u-HA/PLLA) composite for application in spinal interbody fusion cages [6]. Tsou *et al* reported the preparation of a radiolucent cage by using hydroxyapatite grafts[7]. Atiprayoon *et al* reported the preparation of titanium cage with hydroxyapatite [8]. Lu *et al* prepared a poly(propylene fumarate)-hydroxyapatite nanocomposite for application in fusion cages[9]. Quan *et al* reported the preparation of nano-hydroxyapatite/polyamide 66 composite for treatment of cervical spondylotic myelopathy[10]. Although hydroxyapatite-based intervertebral fusion cages have been reported, yet, it still exists poor processability, insufficient biocompatibility and lack of comfort due to high hardness. Therefore, it is still an ambitious challenge to fabricate biocompatible and comfortable intervertebral fusion cage based on hydroxyapatite. On the other hand, graphene nanosheets have been applied in bone regeneration due to its excellent biocompatibility, large surface to volume ratio and excellent antibacterial performance[11]. Unfortunately, there are rare reports on the application of graphene in intervertebral fusion cage.

In this study, we developed a novel hydroxyapatite/graphene/PVA composite for improving biocompatibility, osteoconductivity and comfort of intervertebral fusion cage. The resulting composite exhibits elasticity and soft, reducing the interface pressure between the bone and the implant. All compositions are biocompatible materials with little or no biotoxicity. The hydroxyapatite is conducive to the rapid growth of bones, and graphene has a good bactericidal effect and can avoid causing inflammation. The work thus opens a new avenue for the design and fabrication of high-performance fusion cages.

Experimental section

Materials

Polyvinyl alcohol (PVA1788) was purchased from Hubei Xinkang Pharmaceutical chemical Co., LTD. Citric acid was purchased from Damao Chemical Reagent Co., Ltd. Chitosan, Calcein and fumed silica (99.8%, 200m^2/g) were purchased from Macklin. Triethanolamine was purchased from Tianjin Beichen Fangzheng Reagent Factory. Hydroxyapatite (96%, 60nm) and Polyvinylpyrrolidone (K30) were purchased from Nanjing Duly Biotechnology Co., Ltd. Phosphoric acid buffer (0.1M, pH=7.4) was purchased from Howei Pharm. All chemical were used as received without further purification.

Preparation of elastic fusion cage

Polyvinylpyrrolidone@graphene (PVP@G) was prepared according to previous work[12]. 15g $KMnO_4$ was added to 90mL concentrated sulfuric acid in the ice bath. 15g natural graphite was added to above solution under mechanical stirring at room temperature for 1.0h. Then, above mixture was added to 60g Na_2CO_3 under mechanical stirring. 210mL H_3PO_4 was added into above mixed system under mechanical stirring for 5.0h. Thereafter, the products were washed and filtered, forming expanded graphite (EG). 5g EG and 10g PVP were added to 500mL NaOH solution (pH=14). The mixture was mechanical agitation for 2.0h at 15,000 rpm by using an FA 40 high shear dispersing emulsifier (Fluko), forming PVP@G dispersion solution. The PVP@G powders were obtained by thermal drying process.

The elastic fusion cage was prepared by a facile three-steps as shown in following. Firstly, a cage mold was fabricated by 3D printing technology. It contains with anti-skid teeth on the end face with a length, width and height of 15.5mm× 13mm×8mm and a slope of 7.0º. Secondly, 10g PVA was dissolved into 90.0g deionized water under mechanical stirring at 93.0°C. And then, citric acid, chitosan (CA) and triethanolamine were added to above PVA aqueous solution under mechanical stirring for 10min. Silica and hydroxyapatite were further added to above mixture under mechanical stirring for 30.0min. In a comparison, the PVP@G powders were added to above mixture under mechanical stirring and ultrasonic for 30min. Thirdly, the final blend was loaded into the 3D printing mold. The mold was frozen for 6h and then freeze-dried at -40.0°C for 12h by using a vacuum freeze dryer (LGJ-10). The elastic fusion cage was obtained by removing the mold.

Characterization

The crystal structure of samples was characterized by using XRD diffractometer (TD 3500, china) with a Cu Kα radiation diffraction (λ=0.154nm, 35.0kV, and 40.0mA).

The chemical structure of samples were recorded by a Fourier transform infrared (FT-IR) spectrometer (Thermo Nicolet 360) in the range of 4000-500 cm^{-1}.

The micro-structure and the element distribution of the samples were observed by field emission scanning electron microscope (SEM, Phenom-XL) with energy disperse spectroscopy (EDS).

The mechanical properties of all samples were characterized by compression and tensile tests. In the uniaxial compression test, a rectangle sample with a length, width and thickness of 10mm × 10mm × 8mm was used, and the compression rate was 2mm/min. In the tensile test, the rectangle sample with a length, width and thickness of 115mm×6mm×8mm was used, and the elongation at fixed elongation was 50mm/min.

Water absorption rate was determined as follows. The sample was soak in phosphoric acid buffer (PBS) at ambient temperature for 9h. The sample was then taken out of the buffer and weighted every one hour. The water absorption rate was calculated by equation (1):

$$\text{Water absorption ratio} = \frac{M_0 - M_s}{M_s} \times 100\% \qquad (1)$$

Where M_s and M_0 are the mass of the dried and wet cage (t=0), respectively.

The bone regeneration ability of fusion cage was also characterized as follows. 0.025g calcein was dissolved in pure PBS (50mL), forming fluorescent indicator. The fusion cage was immersed in PBS for 9.0h and then took from the buffer. 0.1mL buffer and 0.1 mL fluorescent indicator were mixed for 3.0min and characterized by fluorescence microscope (TM680).

The agar diffusion test was conducted to evaluate cytotoxicity as show in following. L-929 cells were coated on MEM medium containing 10% fetal bovine serum, which were further cultured in 5% CO_2 and 37℃ incubator. Cells were dispersed in fresh medium and adjusted to 2.5×10^5 cells/ml cell suspension. The above cell suspension was inoculated into a 6-hole plate (2ml/hole), and then was further cultured in a 37℃ and 5% CO_2 incubator for 24 hours. 2% sterilized agar and 2% FBS×MEM culture medium is mixed at 48℃ in equal volume. The above mixture was added to 6-hole plate (2ml/hole) after removing original culture medium and solidified at room temperature. The testing sample, negative and positive sample were
tightly stuck on surface of solidified agar and cultured in a 37℃ and 5% CO_2 incubator

for 24 hours. Finally, the samples were removed from surface of solidified agar in the 6-hole plate. The 0.01% neutral red dye solution was added into each hole and incubated in dark at 37℃ for 1 hour. The surface of solidified agar was observed by a microscope after removing neutral red dye solution.

Results and discussion

A new elastic fusion cage is designed and developed, which is composed of PVA, chitosan(CA), citric acid, hydroxyapatites (HAp), PVP modified graphene nanosheets (GNs), triethanolamine and silica particles. Using citric acid as non-toxic cross-linker, esterification reaction of OH groups of PVA and chitosan is carried out (as chemical crosslinks) by self-exothermic esterification-crosslinking method (Fig.1A)[13-14]. In a comparison, the PVA/CA composite cannot retain their origin shape after freeze-drying in absence of citric acid, suggesting a low degree of cross-linking (Fig.1B). In addition, during the freeze-drying process, the long PVA chains will form crystalline domains (as physical cross-links) in composite (Fig.1A). The HAp and GNs dispersed in the matrix can promote bone growth and improve the mechanical stability and antibacterial property of the composite, respectively. Inorganic silica particles can increase the mechanical strength of the composite, while triethanolamine can effectively improve the dispersion of HAp and GNs in the composite. The formation of HAp/GNs/CA-PVA composite was confirmed by the XRD, Raman and IR spectra. Five diffraction peaks at 26.0°, 32.2°, 40.0º, 47.1º and 49.7° were observed, corresponding to the (002), (211), (310), (222) and (213) crystal planes of hydroxyapatite (JCPDS No 09-0432) (Fig.1C)[15]. From the Raman spectra, the sample without GNs showed a relatively smooth profile (Fig.1D-b). In contrast, two peaks at 1345.0cm^{-1} and 1581.0cm^{-1} were observed for the HAp/GNs/CA-PVA composite (Fig.1D-a), corresponding to characteristic D and G band of graphene, respectively[9]. From FT-IR spectra, the two absorption peaks at 3571.0cm^{-1} and 1047.0cm^{-1} were assigned to -OH and PO_4^{-3} of hydroxyapatite, respectively (Fig.1E-a). The absorption bands at 3490cm^{-1} and 1650.0cm^{-1} were assigned to -OH and O-C groups of chitosan, respectively (Fig.1E-b). The absorption bands at 3450cm^{-1} and 1450.0cm^{-1} were assigned to -OH and C-N groups of TEOA, respectively (Fig.1E-c). The absorption bands at 1710cm^{-1} and 3450.0cm^{-1} were assigned to -C=O and -OH groups of citric acid, respectively (Fig.1E-d). Above absorption peaks were all observed in the spectra of composite (Fig.1E-e and f). These results demonstrate the successful fabrication of HAp/GNs/CA-PVA composite.

Figure 1.

The structure of present fusion cage based on HAp/GNs/CA-PVA was characterized and analyzed as shown in Fig.2. The fusion cage has a sawtooth structure with width, length, and slope of 1.5mm, 3.1mm and 26^{o} (Fig.2A). The surface of sawtooth exhibited a convex-concave structure with a width and depth of 0.4mm and 0.2mm (Fig.2A). These structures can be fabricated by 3D printing technology. As shown in inset of Fig.2B and 2C, the fusion based on HAp/CA-PVA and HAp/GNs/CA-PVA are white and black, respectively. The micro-structure of HAp/CA-PVA and HAp/GNs/CA-PVA was firstly characterized and compared by three-dimensional stereoscopic diagram (Fig.2B-C), which showed a similar surface roughness of 0.6μm and 0.4μm, respectively. The micro-structure of HAp/CA-PVA and HAp/GNs/CA-PVA was also characterized by the SEM images. It also clearly exhibited high surface roughness, resulting from assembly of flower particles (Fig.2D-E). The flower particles were assembly of sheets (inset of Fig.2E). These results demonstrated the formation of fusion cages with hierarchical structures, which is key to preventing slippage between cages and bone[16-17]. The hierarchically rough surface structure of HAp/GNs/CA-PVA composite is more favorable for cell attachment and proliferation of *in vivo* experiments[20-21]. Through element mapping analysis (inset of Fig.2D-E), we clearly identified *P* and *Ca* elements, indicating that the flower-like spherical particles were assigned to hydroxyapatite. In addition, it was also found that both samples showed compact structures due to high solids content (Fig.2D-E). In contrast, conventional hydroxyapatite-based composites have porous structures, as hydrogels mostly shrink or break after thermal drying[14, 18-19].

Figure 2.

The compressive mechanical property of the fusion cages was firstly characterized as shown in Fig.3A. The two samples showed similar compressive stress-strain curves without a significant yield point. The maximum compressive strength of HAp/CA-PVA and HAp/GNs/CA-PVA composite was about 10.7MPa and 6.1MPa, respectively. The compressive strength of the fusion cages is higher than pressure (0.1~1.5MPa) of intervertebral disk[23]. In addition, the compressive stress-strain curves of two samples exhibited linear elastic deformation in lower strain region than 15%. The elastic compressive deformation of interbody fusion cage is benefit to move for the intervertebral disk, which is difficult to realize in commercial interbody fusion cage based on Ti metal, PEEK plastic and so on[24]. The tensile stress-strain curves of two

samples were also characterized and compared as shown in Fig.3B. The elastic modulus of HAp/CA-PVA and HAp/GNs/CA-PVA composite was *ca.* 24.6 MPa and 246.5MPa, respectively. The maximum tensile strength of HAp/CA-PVA and HAp/GNs/CA-PVA composite was about 1.8MPa and 0.9 MPa, respectively. The values are close to human articular cartilage (>0.5MPa)[25]. In a comparison, the HAp/CA-PVA composite showed higher compressive strength and higher tensile strength compared with HAp/GNs/CA-PVA composite. This result may be attributed to the incorporation of graphene nanosheets, limiting the formation of cross-links between CA and PVA. In addition, the two fusion cages displayed small water contact angle of *ca.* 40º (Fig.3C), indicating their super-hydrophilicity. This is also the key to the extend and grow of related cells [22]. These results show that the prepared elastic fusion cages have the potential to replace the intervertebral disc in the corresponding position to achieve the buffer force.

Figure 3.

The ability of the fusion cage to promote bone growth was further evaluated. Fig.4A shows the water absorption performance of the fusion cages. The maximum water absorption ratio of HAp/CA-PVA and HAp/GNs/CA-PVA composite was 38.8% and 53.7%, respectively. Due to the low cross-linking density, the HAp/GNs/CA-PVA composite achieved greater water absorption ratio, which could guide the construction of extracellular matrix and promote cell adhesion and bone growth[22]. Fig.4B shows the XRD pattern of fusion cage after immersing in PBS solution. Some diffraction peaks were clearly observed, which were assigned to CaP_2O_6 (PDF #11-0039). This result indicates that calcium ions can easily be precipitated from the fusion cage. These free calcium ions can regulate the proliferation and differentiation of various cells (such as osteoblasts, osteoclasts, etc.) in the bone repair stage, thereby promoting growth of bone [26-27]. Above result was further confirmed by the fluorescence microscopy images (Fig.4C-D). We could observe a lots of Ca ions from the PBS solutions after fusion cage was immersed. In addition, the cytotoxicity of HAp/GNs/CA-PVA composite was further characterized by agar diffusion method (in Fig.4E). The grades 0 (no reactivity) to 4 (severe reactivity) are generally used to evaluate the cytotoxicity[28-29]. In a comparison with negative sample (Fig.4F), biological reactivity (cellular degeneration and malformation) was not observed around HAp/GNs/CA-PVA composite, indicating low reactivity (grade 1). Generally, the grade of cytotoxicity is smaller than 3, indicating that the bio-material is no harm to human. These results confirm the good

biocompatibility of HAp/GNs/CA-PVA composite, which can be applied in human.

Figure 4.

Conclusions

In this study, a new soft interbody fusion cage was prepared by combining a self-exothermic esterification-crosslinking method with 3D printing mold. Furthermore, the fusion cage shows appropriate elastic and soft property, reducing the risk for infection and improving human comfort. In addition, the prepared fusion cage has a desirable hierarchical structure that provides space for the related cells to extend and grow toward the implant. It can induce the formation of hydroxyapatite, indicating good bio-active performance. This work thus provides a new method for designing and fabricating high performance interbody fusion cage for practical applications.

Acknowledgments

The authors are grateful for the support of the National Natural Science Foundation of China under grants (51773184), Natural Science Foundation of Shanxi Province (201803D421081 and 20181102014).

Conflict of interest

The authors declared that they have no conflicts of interest to this work.

Data availability

Data sharing not applicable to this article as no datasets were generated or analyzed during the current study.

References

1. G.Matge: Cervical cage fusion with 5 different implants: 250 cases. *Acta Neurochir*. 144, 539(2002).

2. G.Bartosz, and D.Maciej: Advantages and Disadvantages of the Use of Various Types of Interbody Implants in Cervical Spine Surgery. Critical Review of the Literature. *Ortopedia traumatologia rehabilitacja*. 12, 213 (2020).

3. S.A.Zadegan, A.Abedi, H.N.Bonaki, A.R.Vaccaro, V.R.Movaghar, and S.B.Jazayeri: Clinical Application of Ceramics in Anterior Cervical Discectomy and Fusion: A Review and Update. *Global Spine Journal*. 7, 343(2017) .

4. X.Yang, Q. Chen, L.M.Liu, Y.M.Song, Q.Q.Kong, J.C.Zeng, Y.D.Xue, C.P.Ren: Comparison of anterior cervical fusion by titanium mesh cage versus nano-hydroxyapatite/polyamide cage following single-level corpectomy. *Int Orthop*. 37, 2421(2013) .

5. C.Brenke, S.Kindling, J.Scharf, K.Schmieder and M.Barth: Short-term experience

with a new absorbable composite cage (beta-tricalcium phosphate-polylactic acid) in patients after stand-alone anterior cervical discectomy and fusion. *Spine.* 38, 635(2013).
6. Y. Shikinami, and M. Okuno: Mechanical evaluation of novel spinal interbody fusion cages made of bioactive, resorbable composites. *Biomaterials*. 24, 3161(2003).
7. W.C.Chang, H.K.Tsou, W.S.Chen, C.C. Chen, and C.C. Shen: Preliminary comparison of radiolucent cages containing either autogenous cancellous bone or hydroxyapatite graft in multilevel cervical fusion. *J Clin Neurosci*. 16, 793(2009).
8. P.Tienboon, and S.Atiprayoon: Comparing anterior cervical fusion using titanium cage with hydroxyapatite and with autograft. *Asian Biomedicine*. 4, 147 (2010).
9. Y.Teng, G.Hugo, R.Asghar, X.Liu, M.A.Lee, B.E.Waletzki, and L.Lu: Poly(Propylene Fumarate)-Hydroxyapatite Nanocomposite Can Be a Suitable Candidate for Cervical Cages. *J Biomech Eng*. 140, 221(2018) .
10.Y.Zhang, X.Deng, D.M. Jiang, X.J.Luo, K.Tang, Z.H.Zhao, W.Y. Zhong, T.Lei, and Z.X. Quan: Long-term results of anterior cervical corpectomy and fusion with nano-hydroxyapatite/polyamide 66 strut for cervical spondylotic myelopathy. *Sci Rep*. 6, 26751(2016).
11.Z .Du, C.Wang, R.Zhang, X.Wang, and X Li: Applications of Graphene and Its Derivatives in Bone Repair: Advantages for Promoting Bone Formation and Providing Real-Time Detection, Challenges and Future Prospects. *Int J Nanomedicine*. 15, 7523 (2020) .
12.H.Y. Zheng, R.H.Guan, Q..X.Liu, K.T.Ou, D.S.Li, J.Fang, Q.Fu, and Y.Y.Sun:A flexible supercapacitor with high capacitance retention at an ultra-low temperature of -65.0℃. *Electrochimica Acta*. 424, 140644(2022).
13.V.S.Ghorpade, R.J.Dias, K.K.Mali, and S. I.Mulla: Citric acid crosslinked carboxymethylcellulose-polyvinyl alcohol hydrogel films for extended release of water soluble basic drugs. *Journal of Drug Delivery Science and Technology*. 52, 421(2019).
14. M.N.A.Wahid, S.I.A.Razak, M.R.A.Kadir, K.A.M.Amin, A. R.S.Izwan, and W.M. N.Abdul:Influence of citric acid on the physical and biomineralization ability of freeze/thaw poly(vinyl alcohol) hydrogel. *J Biomater Appl*. 33, 94 (2018) .
15. J.J.Du, S.C.Gan, Q.H.Bian, D.H.Fu, Y.Wei, K.Q.Wang, Q.X.Lin, W.Y.Chen, D.Huang: Preparation and characterization of porous hydroxyapatite/beta-cyclodextrin-based polyurethane composite scaffolds for bone tissue engineering. *J Biomater Appl*. 33, 402 (2018).
16.T.P. Kunzler, T. Drobek, M.Schuler, and N. D. Spencer: Systematic study of

osteoblast and fibroblast response to roughness by means of surface-morphology gradients. *Biomaterials*. 28, 2175(2007).

17. L.Cao, Q.Chen, L.B.Jiang, X.F.Yin, C.Bian, H.R.Wang, Y.Q .Ma, X.Q.Li, X.L. Li, and J.Dong: Bioabsorbable self-retaining PLA/nano-sized beta-TCP cervical spine interbody fusion cage in goat models: an in vivo study. *Int J Nanomedicine*. 12, 7197(2017).

18.Y.H.Wang, X.F. Cao, M.Ma, W.P. Lu, B. Zhang, and Y.C. Guo: A Gel MA-PEGDA-nHA Composite Hydrogel for Bone Tissue Engineering. *Materials (Basel)* .13, 2(2022).

19. K.Chen, J.L.Liu, X.H.Yang, and D.K.Zhang: Preparation, optimization and property of PVA-HA/PAA composite hydrogel. *Mater Sci Eng C*. 78, 520(2017).

20. Z.Q.Zhang, Z.Q.Ma, Y.H.Zhang, F.X. Chen, Y.Zhou, and Q.An: Dehydrothermally crosslinked collagen/hydroxyapatite composite for enhanced in vivo bone repair. *Colloids Surf B Biointerfaces*. 163, 394(2018) .

21. X.X.Fan, H.T.Peng, H.Li, and Y.G.Yan: Reconstruction of calvarial bone defects using poly(amino acid)/hydroxyapatite/calcium sulfate composite. *J Biomater Sci Polym Ed*. 30, 107(2019).

22.Z.K.Kuo, M.Y.Fang, T.Y.Wu, T.Yang, H.W.Tseng, C.C.Chen, C.M.Cheng: Hydrophilic films: How hydrophilicity affects blood compatibility and cellular compatibility. *Advances in Polymer Technology*. 37, 1635(2018).

23.J.G.McMorran, and D.E.Gregory:The effect of compressive loading rate on annulus fibrosus strength following endplate fracture. *Medical Engineering and Physics*. 93, 17(2021).

24.H.Zhang, Z.H.Wang, Y.Wang, Z.H.Li, B.Chao, S.X.Liu, W.W.Luo, J.H.Jiao and M.F.Wu: Biomaterials for Interbody Fusion in Bone Tissue Engineering. *Frontiers in Bioengineering and Biotechnology*. 900992(2022).

25.K. Liu, L.Zhu, S.Tang, W.Wen, L.Lu, M.Liu, C.Zhou, and B.Luo：Fabrication and evaluation of a chitin whisker/poly(L-lactide) composite scaffold by the direct trisolvent-ink writing method for bone tissue engineering. *Nanoscale*. 12, 18225 (2020) .

26.S.Nakamura, T.Matsumoto, J.I. Sasaki, H.Egusa, K.Y.Lee, T.Nakano, T. Sohmura, and A.Nakahira: Effect of calcium ion concentrations on osteogenic differentiation and hematopoietic stem cell niche-related protein expression in osteoblasts. *Tissue Eng Part A*. 16, 2467(2010) .

27.Y.Yang, and Y.Xiao: Biomaterials Regulating Bone Hematoma for Osteogenesis.

Adv Healthc Mater. 2000726(2020) .
28.K.Seyran, T.Tutku, P.Ozhan, and S.Zeynep: Research into biocompatibility and cytotoxicity of daptomycin, gentamicin, vancomycin and teicoplanin antibiotics at common doses added to bone cement. *Joint Diseases and Related Surgery*.31, 328(2020)
29.C.Hendrich, M.Geyer, D.Scheddin, N.Schutze, J, Eulert, and Thull R: A New Osteoblast Cell Culture System for the Testing of Biomaterials in Accordance with Relevant Standards.*Biomedical Engineering-Biomedizinische Technik*. 41, 278(1996)

Figure 1.(A) Structural schematic diagram of the HAp/GNs/CA-PVA composites. (B) The optical photos of HAp/CA-PVA composites in (a) absence and (b) presence of citric acid. (C) XRD pattern and (D) Raman spectra of soft fusion cage based on (a) HAp/GNs/CA-PVA and (b) HAp/CA-PVA. (E) IR spectra of (a) HA, (b) CS, (c) TEOA, (d) CA, (e) HAp/GNs/CA-PVA and (f) HAp/CA-PVA.

Figure 2.(A) Schematic illustration for hierarchical structure of fusion cage. Three

dimensional morphology of fusion cage based on (B) HAp/GNs/CA-PVA and (C) HAp/CA-PVA. SEM of fusion cage based on (D)HAp/CA-PV and (E) HAp/GNs/CA-PVA. The insets of (B) and (C) are the optical photo of fusion cage based on HAp/CA-PVA and HAp/GNs/CA-PVA. The insets of (D) and (E) are the element map image of flower particles.

Figure 3. (A)Tensile and (B) compressive stress-strain curves of (a) HAp/CA-PV and (b) HAp/GNs/CA-PVA composites. (C) Optical photos of water contact angle for fusion cage based on (a) HAp/CA-PV and (b) HAp/GNs/CA-PVA. The insets of (B) are the optical photos of HAp/GNs/CA-PVA composites under compressive force.

Figure 4. (A)The water absorption ratio of fusion cage based on (a) HAp/CA-PVA and (b) HAp/GNs/CA-PVA. (B)XRD diagram of PBS solution after immersing with fusion cage. Fluorescence microscopes of PBS solution after immersing with fusion cage based on (C) HAp/CA-PVA and (D) HAp/GNs/CA-PVA. Optical microscope images of cells on agar after removing (E) HAp/GNs/CA-PVA composites and (F) negative sample with no cytotoxicity.

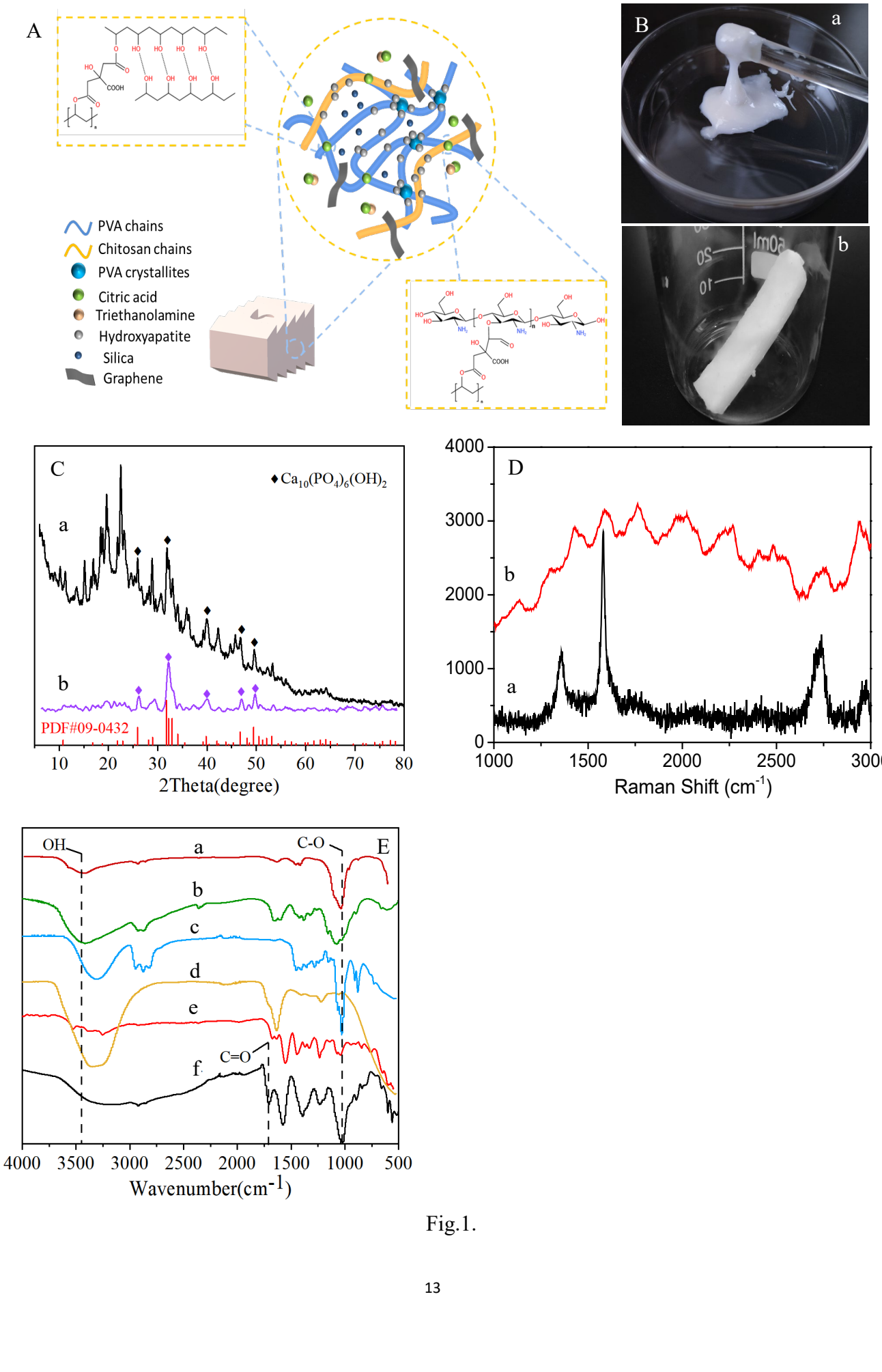
A
PVA chains
Chitosan chains
PVA crystallites
Citric acid
Triethanolamine
Hydroxyapatite
Silica
Graphene
B
a
b
C
♦Ca10(PO4)6(OH)2
a
b
PDF#09-0432
10 20 30 40 50 60 70 80
2Theta(degree)
D
4000
3000
2000
1000
0
b
a
1000 1500 2000 2500 3000
Raman Shift (cm-1)
OH
a
C-O
E
b
c
d
e
f
C=O
4000 3500 3000 2500 2000 1500 1000 500
Wavenumber(cm-1)

Fig.1.

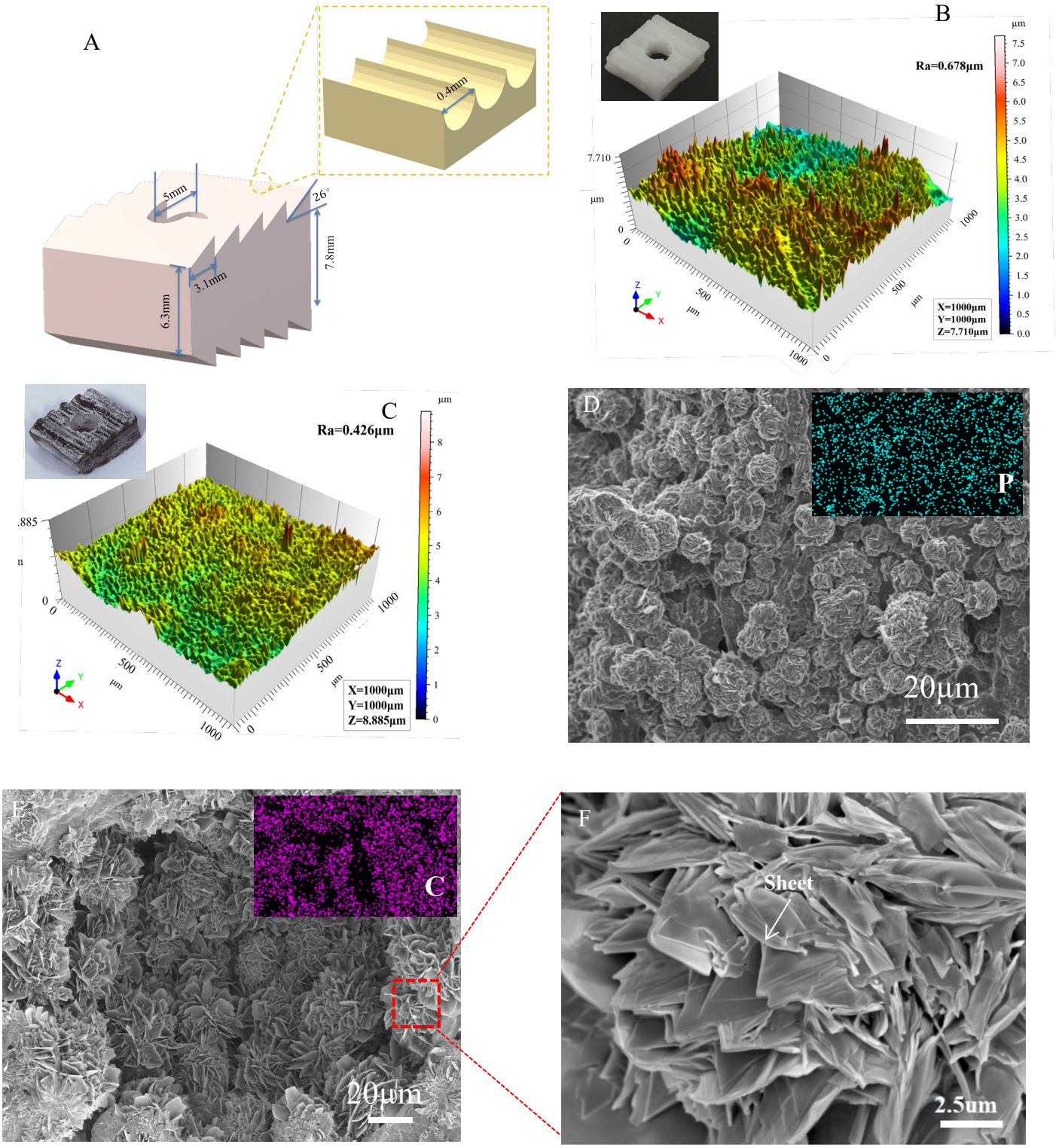
A
0.4mm
5mm
26°
7.8mm
3.1mm
6.3mm
B
Ra=0.678μm
X=1000μm
Y=1000μm
Z=7.710μm
C
Ra=0.426μm
X=1000μm
Y=1000μm
Z=8.885μm
D
P
20μm
E
C
20μm
F
Sheet
2.5um

Fig.2.

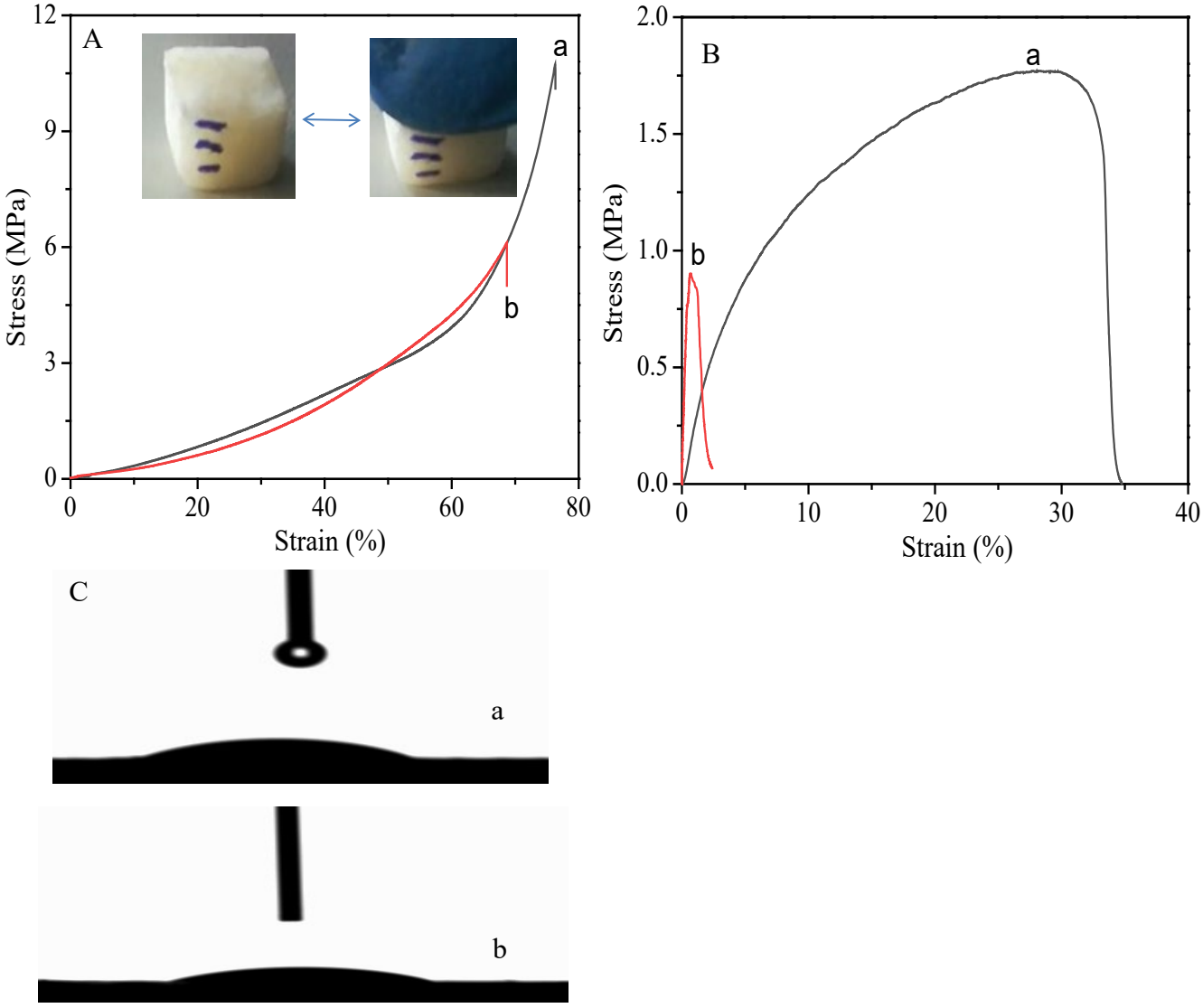

Fig.3.

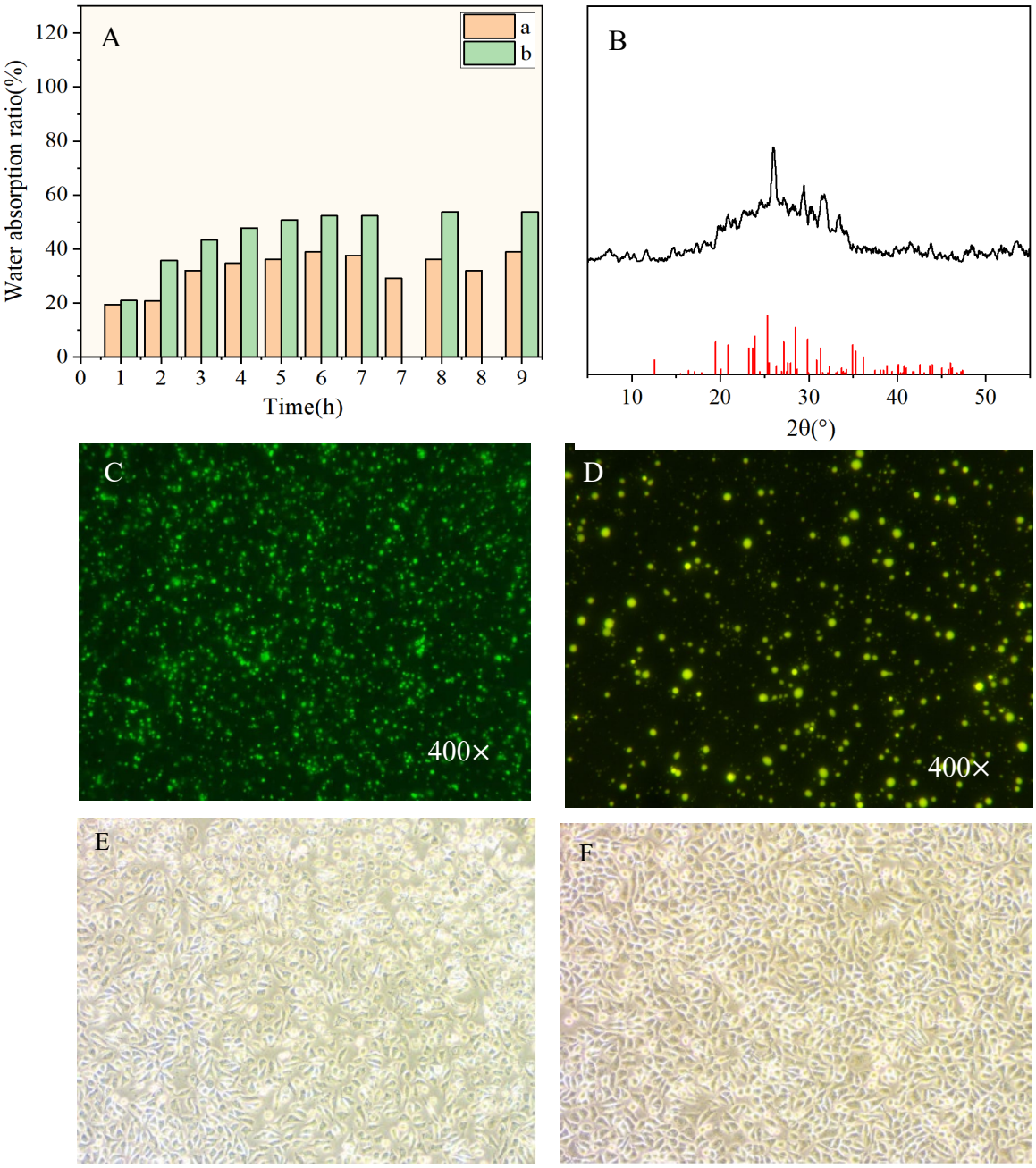

Fig.4.